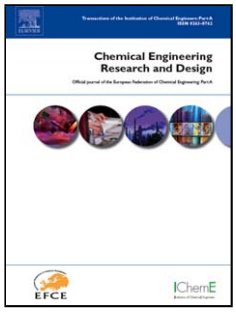

Title: Population balance modelling for a flow induced phase inversion based granulation in a two dimensional rotating agglomerator

Authors: L. Liu, G. Akay, L. Tong

PII: S0263-8762(10)00134-6
DOI: doi:10.1016/j.cherd.2010.04.018
Reference: CHERD 522

To appear in:

Received date: 16-5-2009
Revised date: 23-3-2010
Accepted date: 15-4-2010

Please cite this article as: Liu, L., Akay, G., Tong, L., Population balance modelling for a flow induced phase inversion based granulation in a two dimensional rotating agglomerator, *Chemical Engineering Research and Design* (2008), doi:10.1016/j.cherd.2010.04.018

Population balance modelling for a flow induced phase inversion based granulation in a two dimensional rotating agglomerator

L. Liu[†*], G. Akay[‡] and L. Tong[‡]

[†]Department of Chemical and Process Engineering, University of Sheffield, Mappin Street, Sheffield S1 3JD, UK

[‡]School of Chemical Engineering and Advanced Materials, University of Newcastle, Newcastle Upon Tyne, NE1 7RU, UK

Abstract

A novel two dimensional rotating agglomerator was developed to carry out the flow induced phase inversion (FIPI) based granulation. The process in this agglomerator shows that a continuous paste flow (mixed with liquid binder and primary particles) is extruded into the interstice of two relatively rotating disks, as the paste becomes solidified due to the loss of heat to the disks, it is then broken into granules by the shearing force imposed by the rotating disk. Experimental measurements have shown that the size of these granules is enlarged along the positive radial direction of the disks. It is also found that these granules contain approximately the same quantity of binder in terms of its volume fraction. The paper thus proposes a population balance (PB) model to describe the growth of the granules by considering a size independent agglomeration kernel. The PB simulated results are found to be well capable of describing the change of the particle size distribution (PSD) of the granules in the radial direction. This study also proposes a velocity profile for the paste flow and attempts to establish a quantitative relationship between the granulation rate and the deformation rate as this would help us understand the mechanism of the agglomeration. It is hoped that this study would be used to improve the design of the agglomerator and to assure the control of the process and the granular product quality.

Key words: Agglomeration, granulation, flow induced phase inversion, population balance

[*] corresponding author, lande_liu@yahoo.co.uk

1. Introduction

1.1. FIPI

FIPI is a flow phenomenon in which a continuous phase turns into a dispersed phase, and correspondingly a dispersed phase turns into a continuous phase when the volume ratio of the continuous phase to the dispersed phase is varied from time to time during flow. In the applications of this mechanism (Akay et al., 1994; Akay et al., 1994), generic processes of the agglomeration of solids and liquids and the emulsification of highly viscous resins were developed. The approach adopted in these FIPI processes represents a fundamental shift from agglomeration and emulsification techniques; i.e., the composition and concentration of the process streams are chosen in such a way that the processing is carried out in a highly viscous state, thus requiring the use of high torque mixing-processing equipment such as extruders and compounders; and the final products were obtained when FIPI occurs.

In order to achieve phase inversion during flow, high deformation rates and stresses should be present, which are obtained in continuous processes and in highly viscous materials. Therefore, these FIPI based techniques can be regarded as process intensifications in structured materials in which the restrictions on the thermodynamic state variables (temperature, composition and concentration) are relaxed by imposing a selective mechanical energy field (deformation state variable) during processing (Akay, 1995).

Previous research (Paul, 1979; Gaylord, 1989) regarding phase inversion was mostly concerned with emulsions of two immiscible liquid phases. Because such systems are thermodynamically unstable, mechanical mixing is mostly required. It was also shown (Lissant, 1974) that the maximum volume fraction of the dispersed phase in an emulsion system could reach 74% before the dispersed phase turned into the continuous phase. However, for a FIPI process that particles are involved, the maximum random packing of rigid, monosize spheres is reduced to 63% (Milewski, 1987; German, 1989). It was also claimed (Wildemuth and Williams, 1984) that dispersions containing solid particles with broad or multimodal size distributions can result in a more efficient

particle packing thus increasing the value of the maximum volumetric packing fraction to above 63%.

The influence of flow on phase inversion in emulsions was investigated (Akay et al., 1995), which showed in an unambiguous manner that both the type (i.e. simple shear or extensional shear) and deformation rate as well as fluid microstructure are important. However, phase inversion in multiple polymer systems is not as well understood as it is in emulsions. The tendency for the high viscosity phase to become the continuous phase has been studied (Nielsen, 1974) in the preparation of inverted composites. It was also suggested (Ghijsels and Raadsen, 1980; Van de Vegt and Elmendorp, 1986) that fluids with finite yield stress, i.e. extremely large viscosity at very low shear rates, tend to form the continuous phase at small concentrations. These studies have shown that for a FIPI process especially with high viscosity, mixing conditions and energy dissipation determine when the phase inversion takes place, which is critical to obtain the desired products.

1.2. FIPI based agglomerations

The application of FIPI to the agglomeration of powders was studied (Akay et al., 1998) with aluminium oxide as the primary particles and polyethylene glycol (PEG) and citric acid acting as the coating materials. It was suggested that the phase volume of powders at phase inversion is related to the binder molecular weight as well as the processing conditions.

Based on the understanding of FIPI, a two dimensional rotating agglomerator was developed (Akay, 2000; Akay et al., 2002). This technique is operated under nonisothermal conditions, in which the granules are obtained from a melt fill binder well mixed with primary particles. When the melt fill is going through the equipment with nonisothermal control, the granules at the nuclei stage are formed from the solidification of the melt fill under deformation. Then these nucleated granules start growing with the flow produced by the centrifugal pressure and the pumping from an extruder. The phase inversion occurs from a binder continuous state to a granule continuous state.

The work presented in this paper is concerned with the growth of the granules in such a technique using a steady state PB modelling to describe the change of PSD in radial direction. A

velocity profile of the paste and particle flow is thus proposed to establish the PB equation and to introduce a stress induced mechanical deformation rate into the granulation rate for the interpretation of the stress energy dependence of the agglomeration process.

1.3. PB modelling

PB modelling has been widely used in describing the change of PSD in particulate processes. The PB equation was originated from the work of von Smoluchowski (1917) and then properly derived and analysed by Hulbert and Katz (1964). PB modelling has been applied to describing many aspects of crystallisation (Randolph and Larson, 1988), granulation and other particulate processes (Hounslow, 1998; Ramkrishna, 2000).

The PB equation is a continuity equation allowing a statistical description of particle processes in which the properties of a group of particles change with time and positions. These properties are frequently some measure of particle size and number of particles. In most of cases, there is no analytical solution to the equation; therefore, numerical methods are required (Ramkrishna, 2000). A discretisation technique was developed using the finite difference method (Hounslow et al., 1988; Hill and Ng, 1995) and is the technique used in this paper to produce the PB simulated PSDs in a Mathematica package (DPB, Hounslow, University of Sheffield).

2. Experimental

2.1. Model of the processing unit

The processing unit is shown in Fig. A of the appendix and can also be found in the publication of Akay et al. (2002). Fig. 1 shows a model of the main processing unit of the equipment based on which the velocity profile and PB modelling can then be established.

(Fig. 1)

In Fig. 1, R (=15cm) is the radius of the two disks. The top disk is fixed and the bottom disk is rotating with an angular velocity ω. The gap between the two disks is $2b$ (b=3.75mm). In the centre of the top disk, there is a cylindrical entry with radius r_0 (=7mm) for the paste to be extruded and to flow into the space between the two disks with the rate of the flow denoted as Q.

2.2. Materials and experimental setup

a. The mass mean size of the primary particles (Durcal, component: $CaCO_3$) in diameter is 2.7μm with density 2700 kg m^{-3}.

b. PEG with molecular weight 10000 Da and density 1100 kg m^{-3} as the binder.

c. The mass ratio of the primary particles to the binder is 3:1 (55:45 in volume ratio).

d. The speed of the rotating bottom disk was $\omega = \pi$ rad s^{-1}.

e. The volumetric flow rate of the paste was set to be $Q_1 = 4.8\times10^{-7}$ m^3 s^{-1} and $Q_2 = 7.2\times10^{-7}$ $m^3 s^{-1}$.

2.3. Production of granules

A well-mixed and steadily extruded paste flow passes through the entry cylinder of the top disk and reaches the bottom disk. With the shearing force imposed by the rotation of the bottom disk, the paste flows radially and tangentially in the space between the two disks. Due to the difference of the temperature between the paste and the disks, the convective heat transfer takes place from the paste to the disks while the paste is flowing radially from the middle to the edge of the disks. When the temperature of the paste drops to the solidification point, the paste starts to break up into the nucleus granules. Fig. 2 shows the temperature region where the pastes become solidified for different mass contents of PEG10000 (Akay et al., 2002).

(Fig. 2)

As can be seen from Fig. 2, for the paste with 25% mass content of PEG10000, the temperature span of the solidification from start (10 wt% of paste solidified) to completion of (95 wt% of paste solidified) is about 5°C from 48°C to 43°C. This temperature range allows the paste to solidify (before phase inversion) in a transition state (being solidified but not completely solidified) so that when the granular nuclei are produced (after the phase inversion) these nuclei can still agglomerate. Thus, the temperature of the paste when it is flowing into the central entry of the top disk is set to be 70°C. The temperatures for the top and bottom disks are set to be 52°C and 45°C, respectively. As the temperature of the paste is controlled by the two disks after it entered into the interstice between the two disks and the paste is still kept in its transition state, it is thus thought the viscosity

of the binder in the temperature range controlled by the disks does not change significantly therefore does not have large impact on changing the agglomeration rate of the granules. It was found that there was a paste area around the centre of the bottom disk after phase inversion occurred and granular nuclei are produced. The radius of the paste area is measured and found to be 9cm for Q_1 but 10.4cm for Q_2. The granules for Q_1 were collected and sampled at r = 9.0cm, 10.4cm, 11.5cm, 12.5cm and 14.0cm, respectively; nevertheless, for Q_2 they were collected at r = 10.4cm, 11.5cm, 12.5cm and 14.0cm, respectively. The size distributions of these samples were then measured using Camsizer (Retsch Technology, 2000).

2.4. Measurements and results

2.4.1. Total number and mass mean size of granules

Two sets of results as shown in Fig. 3 were obtained after the Camsizer measurement for Q_1 and Q_2, respectively.

(Fig. 3)

In Fig. 3, the Zeroth Moment, m_0 with unit kg^{-1}, means the total number of granules per unit mass. The Moment is defined as:

$$m_j(r) = \int_0^\infty l^j n(r,l) dl \tag{1}$$

where $n(r, l)$ is the number density of granules with size l in diameter at the position r. So, m_0 is corresponding to the Zeroth Moment. The mean size is defined as:

$$l_{i,j}(r) = \left[\frac{m_i(r)}{m_j(r)} \right]^{\frac{1}{i-j}} \tag{2}$$

The mass mean is $l_{4,3}$. The Moments and the mean sizes were only the functions of radius because of the steady state process.

As can been seen from Fig. 3, the decrease of the total number and the growth of the mean size of granules with radius indicates a process of agglomeration.

2.4.2. Binder distribution in granule size

The binder volume fraction was also calculated according to:

$$\Phi(l) = \frac{V_b(l)}{V_b(l) + V_s(l)} \tag{3}$$

where $V_b(l)$ and $V_s(l)$ are the volumes of the binder and the solid in the granules with size l sampled at position r, respectively.

To measure the volume content of binder for the granules in different sizes, the collected samples at each position r after size distribution measurement with Camsizer were then sieved into 18 size classes from 0.1 to 3.0mm. For these granules in each size class, after their total mass has been measured, they were then taken into a furnace for binder elimination. It was normally a 7-8 hour process for the binder to be burnt out of the granules in the temperature around 450 °C inside the furnace while the primary particles ($CaCO_3$) are not affected. The mass of the granules inside the furnace was monitored, when it remains not changing for several hours, after the furnace cooled down, the granules were then taken out the furnace and their mass was again measured. The difference between the masses before and after the furnace was regarded as the mass of the binder contained in those granules. The volume of the binder can thus be calculated according to its density.

Fig. 4 shows the binder volume fraction contained in granules with size l at different position r.

(Fig. 4)

As can be seen from Fig. 4, the volume content of the binder in different sizes of granules remains almost the same so does to the granules in different positions r. It suggests that the binder was uniformed distributed into the granules during the agglomeration. This is due to the fact that the initial granular nuclei are produced from the breakage of the paste in which the primary particles and the binder are well-mixed before the granular phase is produced.

The slightly higher volume fraction of binder shown in this graph contained in small and large granules was due to the experimental errors. This is because the granules at each position r after sieved, the quantities of small and large granules were only a few grams as can be seen from their

size distribution plots as shown in Fig. 7 of Section 4.1. These few grams of granules caused the errors in measurement after the binder eliminated from the granules in the trend seemingly they have lost more masses than other sizes of granules in the furnace. That is the reason why they looked having slightly higher binder content than others. However, this error should be neglected and the granules should be regarded to contain approximately the same content of binder as they all come from a particle and binder well mixed paste.

3. Theoretical analysis

3.1. The velocity profile

A velocity profile is proposed for the paste and the granular flow induced by the centrifugal pressure and the extrusion as illustrated in Fig. 1. With the cylindrical coordinates as also shown in Fig. 1, the velocities are:

$$u = \frac{3Q}{8\pi br}\left(1-\frac{z^2}{b^2}\right) \tag{4a}$$

$$v = \frac{r\omega}{2}\left(1-\frac{z}{b}\right) \tag{4b}$$

$$w = 0 \tag{4c}$$

where ω is the angular velocity of the bottom disk, and u, v, w are the velocity components in r, θ and z directions. It is worth pointing out that u can not be applied to the situation where $r < r_0$ particularly to $r \to 0$ as the flow at $r < r_0$ is discontinuous. Let $\mathbf{U}$ be the velocity vector and $\{u, v, w\} = \{\mathbf{U}_r, \mathbf{U}_\theta, \mathbf{U}_z\}$, it can thus be proven that:

$$\nabla \cdot \mathbf{U} = 0 \tag{5}$$

and

$$\int_{-b}^{b} 2\pi r u dz = \frac{3Q}{4b}\int_{-b}^{b}\left(1-\frac{z^2}{b^2}\right)dz = Q \tag{6}$$

Eq.s (5) and (6) confirm that the velocity profile satisfies the mass balance.

The deformation rate ε (s^{-2}) (Bird et al., 1960) is:

$$\varepsilon = 2\left[\left(\frac{\partial u}{\partial r}\right)^2 + \left(\frac{1}{r}\frac{\partial v}{\partial \theta} + \frac{u}{r}\right)^2 + \left(\frac{\partial w}{\partial z}\right)^2 + \frac{1}{2}\left(r\frac{\partial u}{\partial r}\frac{v}{r} + \frac{1}{r}\frac{\partial v}{\partial \theta}\right)^2 + \frac{1}{2}\left(\frac{1}{r}\frac{\partial v}{\partial \theta} + \frac{\partial v}{\partial z}\right)^2 + \frac{1}{2}\left(\frac{\partial u}{\partial z} + \frac{\partial v}{\partial r}\right)^2\right] \quad (7)$$

Substituting (4a-c) into Eq. (7) yields:

$$\varepsilon = \frac{9Q^2 z^2}{16\pi^2 b^6 r^2} + \frac{9Q^2\left(1 - \frac{z^2}{b^2}\right)^2}{16\pi^2 b^2 r^4} + \frac{\omega^2 r^2}{4b^2} \quad (8)$$

For this two-dimensional flow (b<<R), the in situ z-averaged deformation rate is:

$$\bar{\varepsilon} = \frac{\int_{-b}^{b} 2\pi r \varepsilon dz}{\int_{-b}^{b} 2\pi r dz} = \frac{3Q^2(8b^2 + 5r^2)}{80\pi^2 b^4 r^4} + \frac{\omega^2 r^2}{4b^2} \quad (9)$$

The plots of $\bar{\varepsilon}$ against r for Q_1 and Q_2 and the plot of $\omega^2 r^2 / 4b^2$ versus r are shown in Fig. 5.

(Fig. 5)

As can be seen from Fig. 5, the three curves are overlapped. This implies that the deformation rate $\bar{\varepsilon}$ largely depends on the shearing force which was represented by the second term of the right hand side of Eq. (9). Thus, (9) can be approximately written as:

$$\bar{\varepsilon} \cong \frac{\omega^2 r^2}{4b^2} \quad (10)$$

3.2. PB modelling

The PB equation in agglomeration form is:

$$\frac{\partial n(V)}{\partial t} + \nabla \cdot (\mathbf{U} n(V)) = \frac{1}{2}\int_0^v \beta_{V-s,s} n(V-s) n(s) ds - n(V)\int_0^\infty \beta_{V,s} n(s) ds \quad (11)$$

where n (kg^{-1} m^{-3}) is the number density of granules, V and s are the volume sizes of granules.

From left to right, the first term of (11) describes the change of the number density of particles V in time and the second term tells the migration rate of particles V in spatial coordinates; the third term gives the birth rate of particles V due to aggregation between particles V-ε and ε; and, the

fourth term describes the death rate of particles V owing to the aggregation between particles V and any sizes of particles.

Note, n in Eq. (11) takes the volume size as a variable. This makes the expression of this equation simpler than that of n taking length size in diameter as a variable such as that in Eq. (1), nevertheless, $n(V)dV = n(l)dl$. It should be noted that n is denoted by its size characteristic only, though it is also the function of time and spatial coordinates. β (kg s^{-1}) is the agglomeration kernel also the function of particle size, time and spatial coordinates.

In this study, because of the steady state process and the two-dimensional model, Eq. (11) can be changed to:

$$\overline{u}\frac{\partial n(V)}{\partial r} = \frac{1}{2}\int_0^v \beta_{V-s,s} n(V-s)n(s)ds - n(V)\int_0^\infty \beta_{V,s} n(s)ds \tag{12}$$

where n and β are now only the function of particle size and r. $\overline{u}$ is the in situ z-averaged velocity of u:

$$\overline{u} = \frac{\int_{-b}^{b} 2\pi r u dz}{\int_{-b}^{b} 2\pi r dz} = \frac{Q}{4\pi b r} \tag{13}$$

3.3. The agglomeration kernel

The agglomeration kernel β must be determined before Eq. (12) can be solved to provide the numerical solution for n. In general, agglomeration kernels are the geometric characteristic of particle collisions and used to calculate the collision rate. The use of the kernels, for instance the application of coalescence kernels for wet granulation PB modelling (Ennis and Litster, 1997; Liu and Litster, 2002), is mostly empirical and depends on the understanding of the practical process and the modeller's experience with PB simulation. As suggested (Sastry, 1975) and now it is widely accepted that β can be split into an inherent agglomeration rate β_0 and a size dependence f; thus for this steady state process, we have:

$$\beta(r,V,s) = \beta_0(r) f(V,s) \tag{14}$$

As can be seen from Fig. 4, the binder can be regarded as uniformly distributed into the granules of different sizes at different positions. This indicates that every individual granule has the same chance to agglomerate with other granules, which means that any size of individual granules have no preference in agglomerating with any other sizes of granules and the same to themselves. This suggests that the agglomeration of the granules in this study may be considered to be size independent. Therefore, we have (12) changed to:

$$\overline{u}\frac{\partial n(V)}{\partial r}=\frac{\beta_0}{2}\int_0^v n(V-s)n(s)ds-n(V)\beta_0\int_0^\infty n(s)ds \tag{15}$$

Integrating this equation on both sides over the domain of variable V from 0 to ∞ yields:

$$\overline{u}\frac{dm_0(r)}{dr}=-\frac{\beta_0}{2}m_0(r)^2 \tag{16}$$

Thus:

$$\frac{d\left(\frac{1}{m_0(r)}\right)}{dr}=\frac{\beta_0}{2\overline{u}} \tag{17}$$

Taking β_0 as a constant, we have:

$$\frac{Q}{2\pi b}\left[\frac{1}{m_0(r)}-\frac{1}{m_0(r_0)}\right]=\beta_0(r^2-{r_0}^2) \tag{18}$$

Let $m_0^*(r)=\frac{Q}{2\pi b}\left[\frac{1}{m_0(r)}-\frac{1}{m_0(r_0)}\right]$, the plots of data ($m_0^*(r)$, r) and the fits to the data are shown in Fig. 6.

(Fig. 6)

As can be seen from Fig. 6, the β_0 values for Q_1 and Q_2 are almost the same, thus β_0 can be regarded as a constant in this study.

4. Results and discussion

Results presented in this section are mainly concerned with the PB modelling prediction in PSD and the granulation rate composed of the inherent agglomeration rate, processing variables and experimental parameters. The PB modelling predicted PSDs are used to compare with that of the

experimental measurements in order to justify the model. The granulation rate is analysed to provide suggestions for controlling the growth rate of granule size through controlling process variables and experimental parameters.

4.1. PB simulation

Taking the determined β_0 values into Eq. (15), the simulation is carried out with an initial PSD to predict the PSDs at other radial positions. The initial PSD is set to be the PSD measured at the outside edge of the paste area, i.e., the PSDs at r = 9.0cm and 10.4cm for Q_1 and Q_2, respectively. Fig. 7 shows the comparison between the simulated and experimental PSDs at different radial positions in the form of mass fraction $lw(l)$ (-) (l is the particle size in diameter and $w(l)$ (m^{-1}) is the mass density of the particles with size l). Also in this figure, the Zeroth Moment and $l_{4,3}$ mean size are compared.

(Fig. 7)

As can be seen from Fig. 7, despite some slight under-predictions in the PSD representation of the experimental data, it is still true to say that the PB simulation can largely predict the change of PSD in r especially from the agreement between the modelling and experimental results for the total number and the mean sizes of granules as shown in the corresponding graphs of this figure.

The under-prediction is due to the peak broadening of the PB modelled PSD. This is because the agglomeration rate is determined by Eq. (18), which is associated with the total number of particles at each position r but not necessarily reflecting the shape of each size distribution; so is the fitted rate value β_0 that does not necessarily contain the information of the PSDs either. However, this is the only method that is practically available to determine the agglomeration rate from experiments. Therefore, the correctness of the PB simulation relies on entirely the PB method itself whether it truly reflects the mechanism of the process.

In addition, the PB simulation started from the initial PSDs which are quite wide distributed in terms of particle size span as the ones seen in Fig. 7 for r = 9.0cm and 10.4cm for Q_1: 4.8×10^{-7} m^3 s^{-1} and Q_2: 7.2×10^{-7} m^3 s^{-1}, respectively. Then, in experiments, as r increased, the PSD experienced a

quite dramatic narrowing in terms of the size span, which has resulted in a large increase of the peak value at the modal size. However, the PB simulation using the agglomeration rate determined by Eq. (18) can only compute the PSDs from the initial ones in a more gradually progressive way, as mentioned above the fitted value β_0 does not contain the shape information of the size distributions. Therefore, compared to that of the experiments, the PB modelled PSDs have slightly wider peak values. However, except for this slightly peak broadening, the PB modelled PSDs have rightly followed the shape development of the experimental PSDs and correctly predicted the change of the mean size and total number of granules at each position *r*.

4.2. The granulation rate and the deformation rate

According to Eq. (17), let:

$$\frac{\beta_0}{2\overline{u}} = \beta_0^* \tag{19}$$

Since β_0 is the inherent agglomeration rate, β_0^* (kg m^{-1}) can be regarded as the granulation rate as its unit indicates that this is the rate related to the radial position of the granules. β_0^* means the successful collision efficiency that leads to granulation in mass scaled by the unit length of the radius.

Substituting $\overline{u}$ in Eq. (19) by expression (13) and taking (10) into account to eliminate the variable *r*, we have:

$$\beta_0^* = \frac{4\pi b^2 \beta_0}{Q\omega}\sqrt{\overline{\varepsilon}} \tag{20}$$

As β_0 can be regarded as a constant, expression (20) thus establishes a relationship between the granulation rate and the deformation rate. It suggests how quick the granules will grow in *r* depends on the deformation rate applied to the granules. Fig. 8 shows the effect of the flow rate on β_0^* by plotting it vs $\overline{\varepsilon}$.

(Fig. 8)

It is shown in Fig. 8 that higher flow rates result in lower granulation rates while increasing the mechanical dissipation (characterised by $\bar{\varepsilon}$) will always enhance the granulation rate.

In fact, β_0^* in Eq. (15) is the effective agglomeration rate that provides a quantitative expression for the agglomeration kernel. It is β_0^* that determines how quick the granules will agglomerate thus to grow in size. Any increase in the value of β_0^* will increase the rate of the granule growth, Eq. (20) suggests that to obtain large granules in a short distance along the radial direction of the disks, a low flow rate may be required and a high angular velocity ω will also be useful as the increase of ω increases $\bar{\varepsilon}$ along with r.

Once all the parameters and variables that make up the β_0^* are fixed, the PSD at any r is entirely predictable thus becomes deterministic. Optimising the design of the agglomerator and the process of the granulation will only require β_0^* to be the basis on how to achieve its maximum value in a practical way. For instance, if the diameter $2R$ of the disks and the rotation speed ω of the bottom disk are fixed, increasing the gab $2b$ between the two disks and reducing the flow rate Q of the paste become the only ways to maximise β_0^* thus to maximise the rate of the granules' growth. However, on one hand, reducing flow rate will increase the processing time thus may not be practically applicable. On the other hand, increasing the gap between the two disks will require larger driving power from the extruder to drive the paste and granules to flow thus results in more energy consumption.

Another example is, if the flow rate Q and the rotation speed ω of the bottom disk are determined, the ways to increase the granule size in the granulation are to increase the gap $2b$ between the two disks and increase the diameter $2R$ of the disks so that the granules have a longer distance to travel in order to grow larger as shown in the predicted mean size graphs (lines) in Fig. 7.

Such information is useful in not only designing the size of the equipment but also in determining the processing variables, e.g. Q and ω for the equipment to provide a particular granule size at a particular position; namely, once the size of the equipment (R and b) and the

processing variables such as Q and ω are determined, the PSD at any r is determined and can be calculated by the PB simulation.

Therefore, to optimise the design of the agglomerator and the agglomeration process will depend on the specific cases and circumstances. Nevertheless, the parameters and variables that make up the granulation rate β_0^* remain in the centre of the discussion.

5. Conclusions

The PB modelling for a FIPI based novel agglomeration process is presented in this paper with a velocity profile that is proposed to describe the flow of the paste and the granules. It is found that using a steady state agglomeration PB model, the PSDs of the granules at different positions along the radial direction can be well represented. It is also found that the inherent agglomeration rate can be regarded as a constant that results in the granulation rate being linearly related to the radial position of the granules. This makes possible establish a relationship between the granulation rate and the deformation rate, which can then be used to interpret such an agglomeration process in a fundamental aspect that the mechanical dissipation provides the energy for the granules to agglomerate. However, the effective way to change the granulation rate is to change the flow rate as the granulation rate is directly related to the radial velocity of the granules which is provided by the radial flow of the granules. It is hoped that these results can be used to improve the design of the processing unit in its size and to optimise the processing variables such as the angular velocity and the flow rate in order to control the final PSD of the granular products at any particular radial positions.

It should be mentioned, although the velocity profile satisfies the mass continuity theoretically, its validity still remains to be examined experimentally. This is an ongoing research being carried out together with the analysis of the heat transfer for the process of paste flow and solidification which leads to the breakup of the paste into the initial granular nuclei.

Acknowledgements

This research was supported by the Engineering and Physical Sciences Research Council (EPSRC) of the U.K. (GR/M58276), AstraZeneca, Carl Stewart Ltd., Syngenta Thermo Haake, and Rosand Precision Ltd. Their support is gratefully acknowledged. The authors would also like to thank Prof. M. J. Hounslow for his valuable suggestions.

Nomenclature

Roman symbols

b	half of the gap between two disks	m
f	size dependence of agglomeration kernel	-
l	particle size in diameter	m
$l_{4,3}$	mass mean size of particles in diameter	m
m_0	the Zeroth Moment	kg^{-1}
m_0^*	$Q[1/m_0(r)-1/m_0(r_0)]/2\pi b$	kg m^2 s^{-1}
n	number density of particles	m^{-3} kg^{-1}
Q	volumetric flow rate	m^3 s^{-1}
r	cylindrical coordinate in radial direction	m
r_0	radius of cylindrical entry in the top disk	cm
R	radius of the disks	cm
s	particle size in volume	m^3
V	particle size in volume	m^3
w	mass density of particles	m^{-1}
z	cylindrical coordinate in vertical direction	m

Vectors

U	velocity vector of paste	m s^{-1}
u	velocity component in r direction	m s^{-1}
$\overline{u}$	z-averaged radial velocity	m s^{-1}

v	velocity component in θ direction	m s^{-1}
w	velocity component in z direction	m^{-1}

Greek symbols

β	agglomeration kernel	kg s^{-1}
β_0	agglomeration rate	kg s^{-1}
β_0^*	granulation rate	kg m^{-1}
ω	angular velocity	rad s^{-1}
ε	deformation rate	s^{-2}
$\overline{\varepsilon}$	z-averaged deformation rate	s^{-2}
θ	cylindrical coordinate in angular direction	m
μ	viscosity of the paste	Pa s

References

Akay, G., 1995, Flow Induced Phase Inversion in Powder Structuring by Polymers. In Polymer Powder Technology, Rosenzweig, N. and Narkis, M. (eds), pp. 542-587. (Wiley, New York)

Akay, G., 2000, Intensive Agglomeration and Microencapsulation of Powders. Internal report, University of Newcastle, Newcastle.

Akay, G., Bhumgara, Z. and Wakeman, R.J., 1995, Self-support Porous Channel Filtration Modules: Preparations and Performance. Chem Eng Res Des, 73: 782-797.

Akay, G., Chapple, A., Garrett, P.R., Knight, P.C. and Yorke, J.W.H., 1994, Detergent powder and process for preparing them. Australian Patent, 651,732.

Akay, G., Garrett, P.R. and Yorke, J.W.H., 1994, Antifoam ingredient. European Patent, 593,441.

Akay, G., Price, V.J. and Chan, S.Y., 1998, Flow Induced Phase Inversion in the intensive agglomeration/ micro-encapsulation of Powders. World Congress on Particle Technology III, Brighton, UK.

Akay, G., Tong, L. and Addleman, R., 2002, Process intensification in particle technology: Intensive granulation of powders by thermomechanically induced melt fracture. Ind Eng Chem Res, 41: 5436-5446.

Bird, R.B., Stewart, W.E. and Lightfoot, E.N., 1960, Transport phenomena. (Wiley and Sons, Inc., New York and London)

Ennis, B.J. and Litster, J.D., 1997, Size enlargement. In Perry's chemical engineering handbook (7th ed), Section 8. (McGraw-Hill, New York)

Gaylord, N.G., 1989, Compatibilizing Agents: Structure and Function in Polyblends. J Macromol Sci, Part A: Pure and Applied Chemistry, A26: 1211-1229.

German, R.M., 1989, Particle Packing Characteristics. (Metal Powder Industries Federation, Princeton, N. J.)

Ghijsels, A. and Raadsen, J., 1980, A collaborative study on the melt rheology of a styrene-butadiene-styrene block copolymer. Pure & Appl Chem, 52: 1359-1386.

Hill, P.J. and Ng, K.M., 1995, New discretization procedure for the breakage equation. AIChE J, 41: 1204-1216.

Hounslow, M.J., 1998, The population balance as a tool for understanding particle rate processes. Kona Powder and Particles, 16: 179-193.

Hounslow, M.J., Ryall, R.L. and Marshall, V.R., 1988, A discrete population balance model for nucleation, growth and aggregation. AIChE J, 34: 1821-1832.

Hulbert, H.M. and Katz, S., 1964, Some problems in particle technology: A statistical formulation. Chem Eng Sci, 19: 555-574.

Lissant, K.J., 1974, Emulsions and Emulsion Technology. (Marcel Dekker, New York)

Liu, L.X. and Litster, J.D., 2002, Population balance modelling of granulation with a physically based coalescence kernel. Chem Eng Sci, 57: 2183-2191.

Milewski, J.W., 1987, Handbook of Reinforcements for Plastics. Milewski, J.V. and Katz, H.S. (eds). (Van Nostrand Reinhold, New York)

Nielsen, L.E., 1974, Mechanical Properties of Polymers and Composites. (Marcel Dekker, New York)

Paul, D.R., 1979. In Polymer Blends, Paul, D.R. and Newman, S. (eds). vol. 2. (Academic Press, New York)

Ramkrishna, D., 2000, Population balances: Theory and applications to particulate systems in Engineering. (Academic Press, San Diego, California)

Randolph, A.D. and Larson, M.A., 1988, Theory of particulate Processes. (2nd ed). (Academic Press, New York)

Sastry, K.V.S., 1975, Similarity size distribution of agglomerates during their growth by coalescence in granulation or green pelletization. International Journal of Mineral Processing, 2: 187-203.

Van de Vegt, A.K. and Elmendorp, J.J., 1986, In Integration of Fundamental Polymer Science and Technology, Kleintjens, L. A. and Lemstra, P. J. (eds). (Elsevier Appl Sci Publisher, London)

von Smoluchowski, M.V., 1917, Mathematical theory of the kinetics of the coagulation of colloidal solutions. Zeitschrift fuer Physikalische Chemie, 92: 129-168.

Wildemuth, C.R. and Williams, M.C., 1984, Viscosity of suspensions modeled with a shear-dependent maximum packing fraction. Rheol Acta, 23: 627-635.

Appendix

(Fig. A**)**

Figure captions

Fig. 1 – Model of the processing unit of the two dimensional rotating agglomerator.

Fig. 2 – The temperature profiles of the solidification of the pastes with different mass contents of PEG10000.

Fig. 3 – The total number and mass mean sizes of the granular samples for Q_1 and Q_2 referring to the flow rates 4.8×10^{-7} m^3 s^{-1} and 7.2×10^{-7} m^3 s^{-1}, respectively. Note, Zeroth Moment (m_0) means the total number of granules in a unit mass and $l_{4,3}$ means the mass mean size of the granules.

Fig. 4 – The volume fraction of binder in granular samples for Q_1 and Q_2 that are corresponding to the flow rates 4.8×10^{-7} m^3 s^{-1} and 7.2×10^{-7} m^3 s^{-1}, respectively. Note, the dots with different shapes are overlapping.

Fig. 5 – Deformation rate versus radius. Note, ω denotes the shearing contribution represented by the second term of the right hand side of Eq. (9). Q_1 and Q_2 are corresponding to the flow rates 4.8×10^{-7} m^3 s^{-1} and 7.2×10^{-7} m^3 s^{-1}, respectively.

Fig. 6 – The plots of and the fits to $m_0^*(r)$ versus r^2 for Q_1 and Q_2 that are corresponding to the flow rates 4.8×10^{-7} m^3 s^{-1} and 7.2×10^{-7} m^3 s^{-1}, respectively.

Fig. 7 – The comparison between the PB simulated and the measured PSDs at different radial positions. The Zeroth Moment and the $l_{4,3}$ mean size are also compared. Note, the curves are the simulation results and the dots represent the experimental measurements. Q_1 and Q_2 are corresponding to the flow rates 4.8×10^{-7} m^3 s^{-1} and 7.2×10^{-7} m^3 s^{-1}, respectively.

Fig. 8 – Effect of the flow rate Q on the granulation rate β_0^* in terms of the deformation rate $\bar{\varepsilon}$. Note, the coordinate values on the vertical axis are β_0^* multiplied by 10^9. Q_1 and Q_2 are corresponding to the flow rates 4.8×10^{-7} m^3 s^{-1} and 7.2×10^{-7} m^3 s^{-1}, respectively.

Fig. A – Diagrammatic illustration of the processing unit of the two dimensional rotating agglomerator.

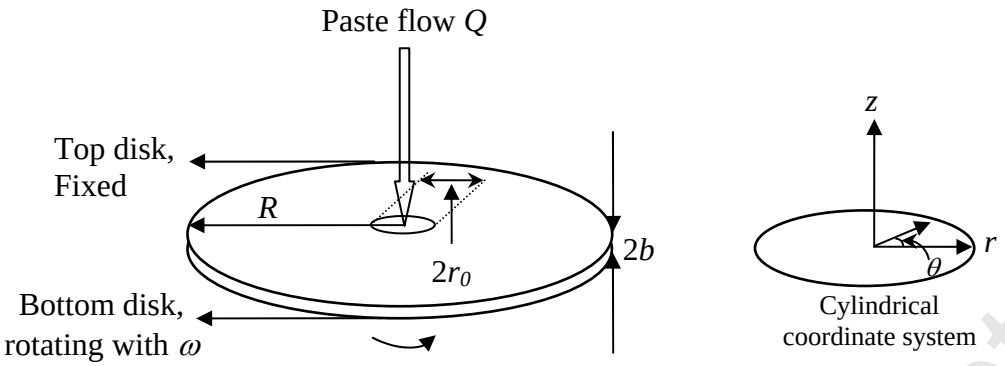

Fig. 1 – Model of the processing unit of the two dimensional rotating agglomerator.

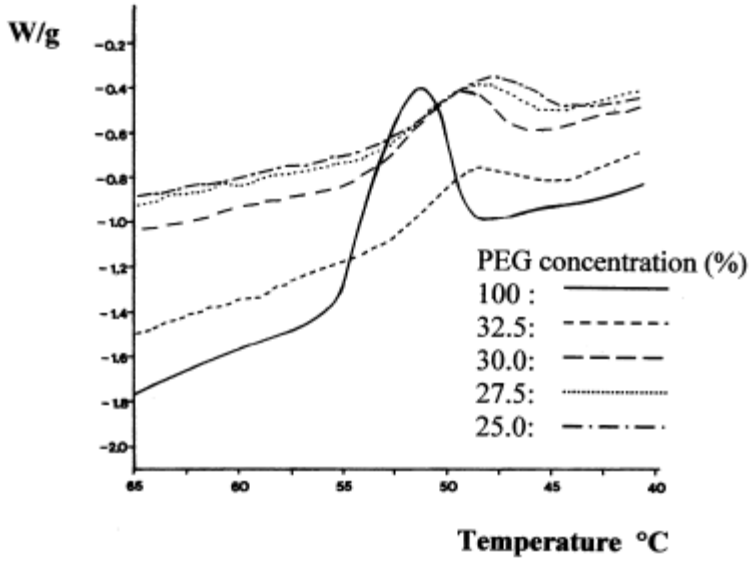

Fig. 2 – The temperature profiles of the solidification of the pastes with different mass contents of PEG10000.

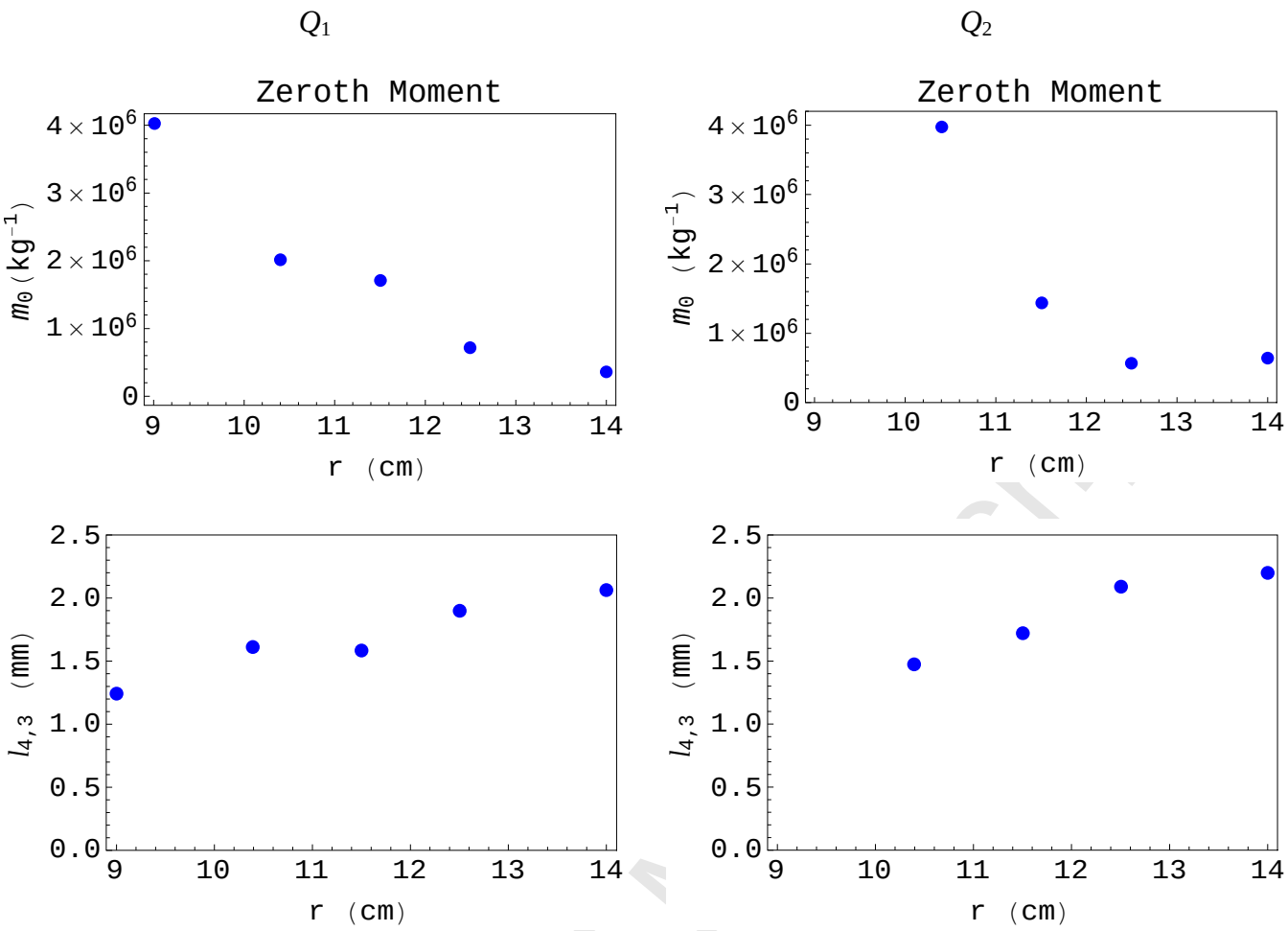

Fig. 3 – The total number and mass mean sizes of the granular samples for Q_1 and Q_2 referring to the flow rates 4.8×10^{-7} m^3 s^{-1} and 7.2×10^{-7} m^3 s^{-1}, respectively. Note, Zeroth Moment (m_0) means the total number of granules in a unit mass and $l_{4,3}$ means the mass mean size of the granules.

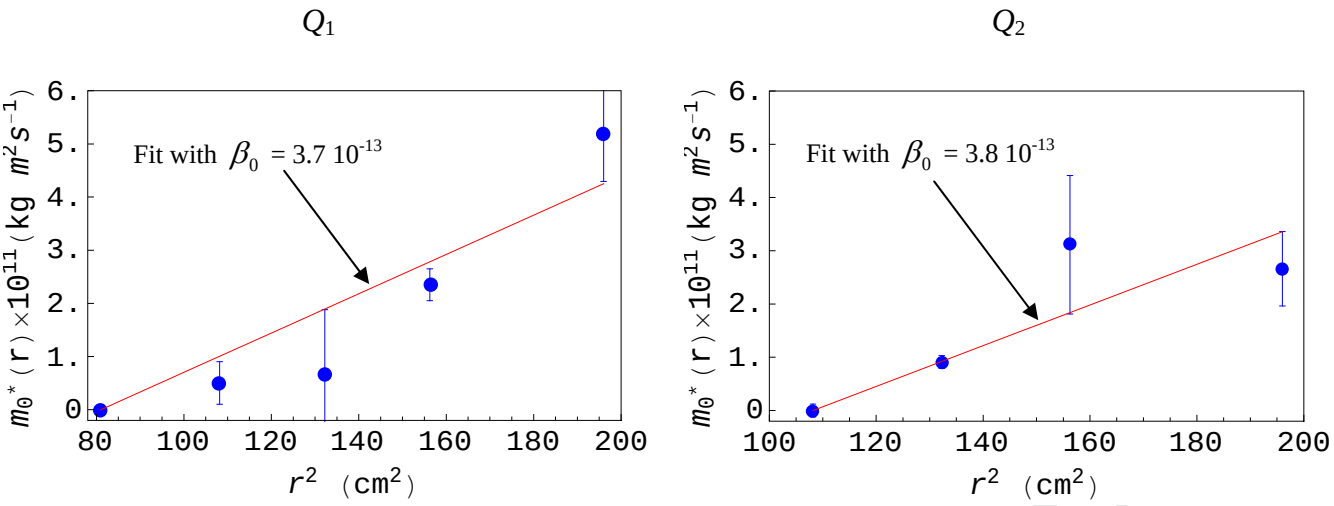

Fig. 6 – The plots of and the fits to $m_0^*(r)$ versus r^2 for Q_1 and Q_2 that are corresponding to the flow rates 4.8×10^{-7} m^3 s^{-1} and 7.2×10^{-7} m^3 s^{-1}, respectively.

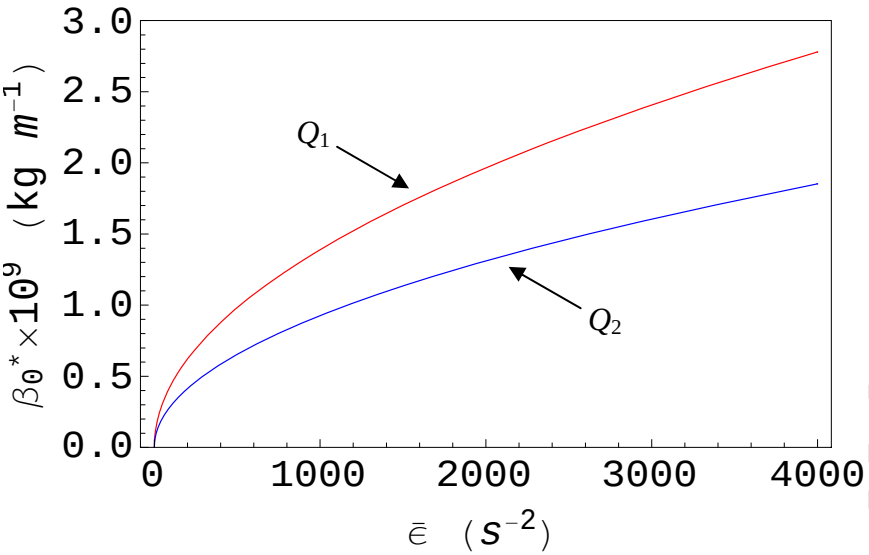

Fig. 8 – Effect of the flow rate Q on the granulation rate β_0^* in terms of the deformation rate $\bar{\varepsilon}$. Note, the coordinate values on the vertical axis are β_0^* multiplied by 10^9. Q_1 and Q_2 are corresponding to the flow rates 4.8×10^{-7} m^3 s^{-1} and 7.2×10^{-7} m^3 s^{-1}, respectively.

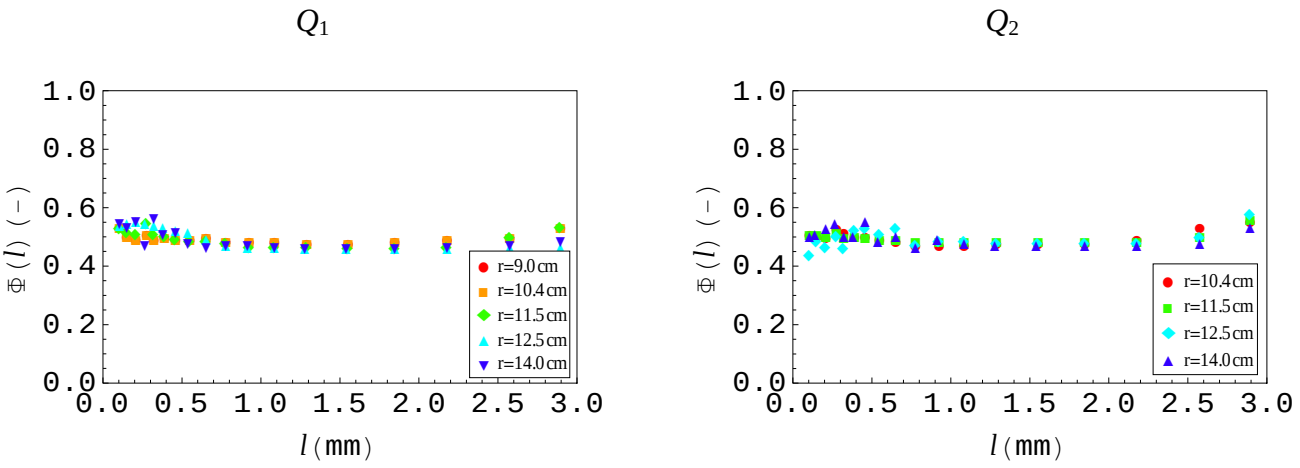

Fig. 4 – The volume fraction of binder in granular samples for Q_1 and Q_2 that are corresponding to the flow rates 4.8×10^{-7} m^3 s^{-1} and 7.2×10^{-7} m^3 s^{-1}, respectively. Note, the dots with different shapes are overlapping.

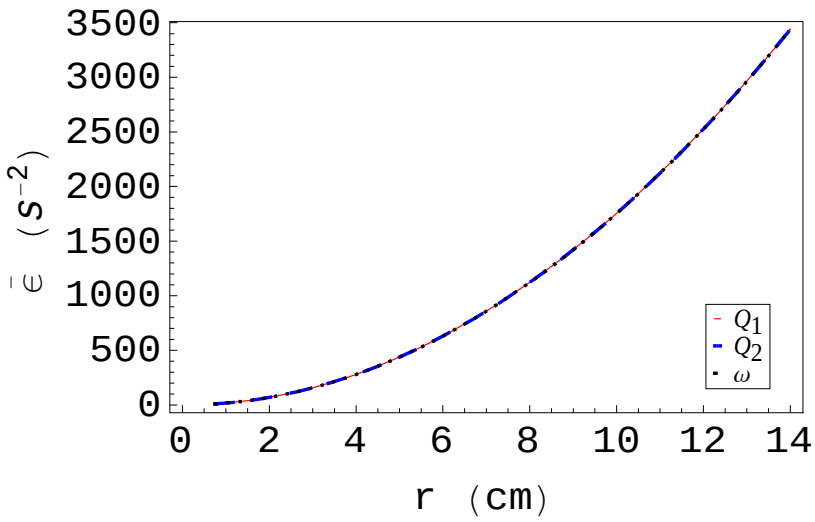

Fig. 5 – Deformation rate versus radius. Note, ω denotes the shearing contribution represented by the second term of the right hand side of Eqn. (9). Q_1 and Q_2 are corresponding to the flow rates 4.8×10^{-7} m^3 s^{-1} and 7.2×10^{-7} m^3 s^{-1}, respectively.

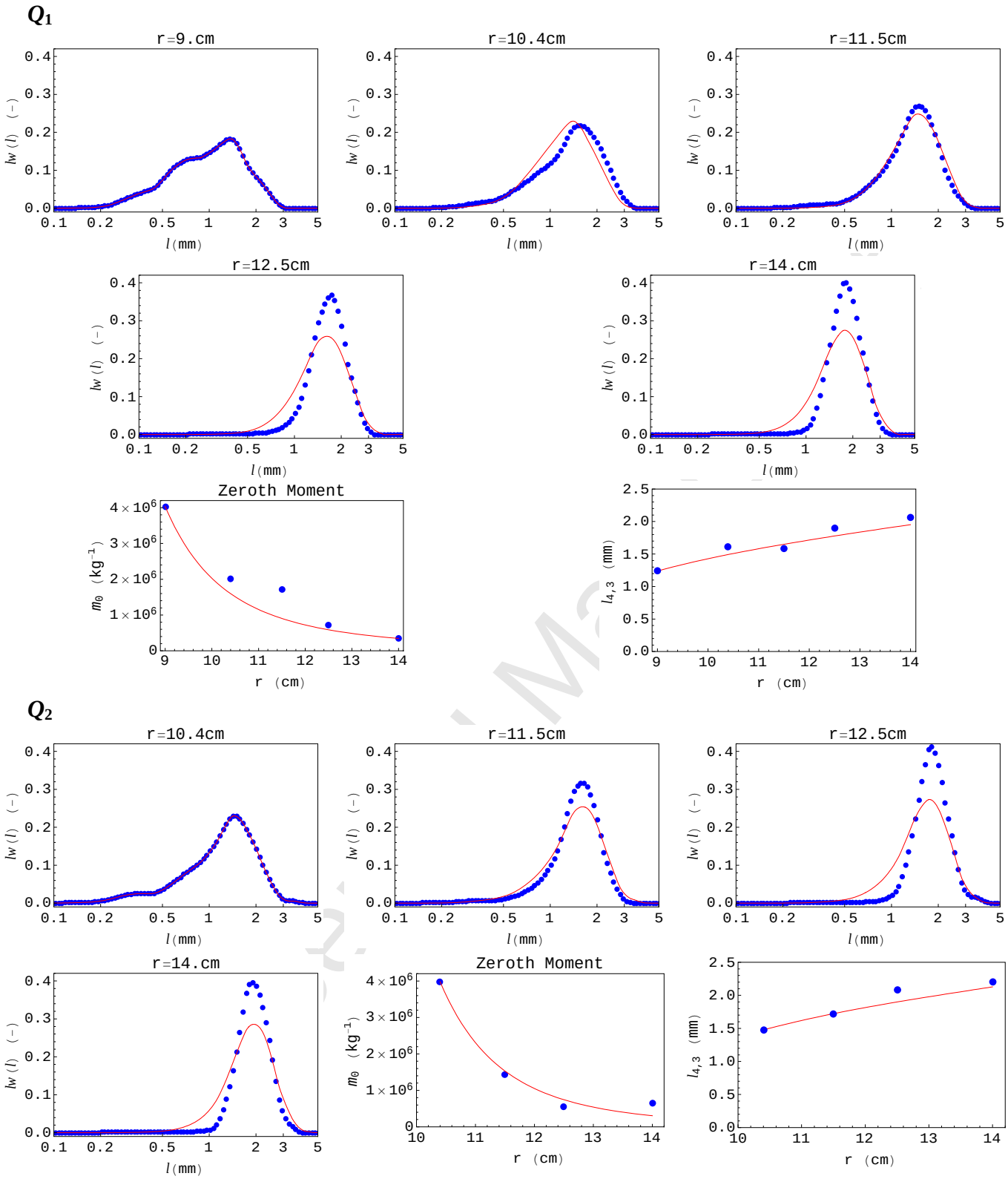

Fig. 7 – The comparison between the PB simulated and the measured PSDs at different radial positions. The Zeroth Moment and the $l_{4,3}$ mean size are also compared. Note, the curves are the simulation results and the dots represent the experimental measurements. Q_1 and Q_2 are corresponding to the flow rates 4.8×10^{-7} m^3 s^{-1} and 7.2×10^{-7} m^3 s^{-1}, respectively.

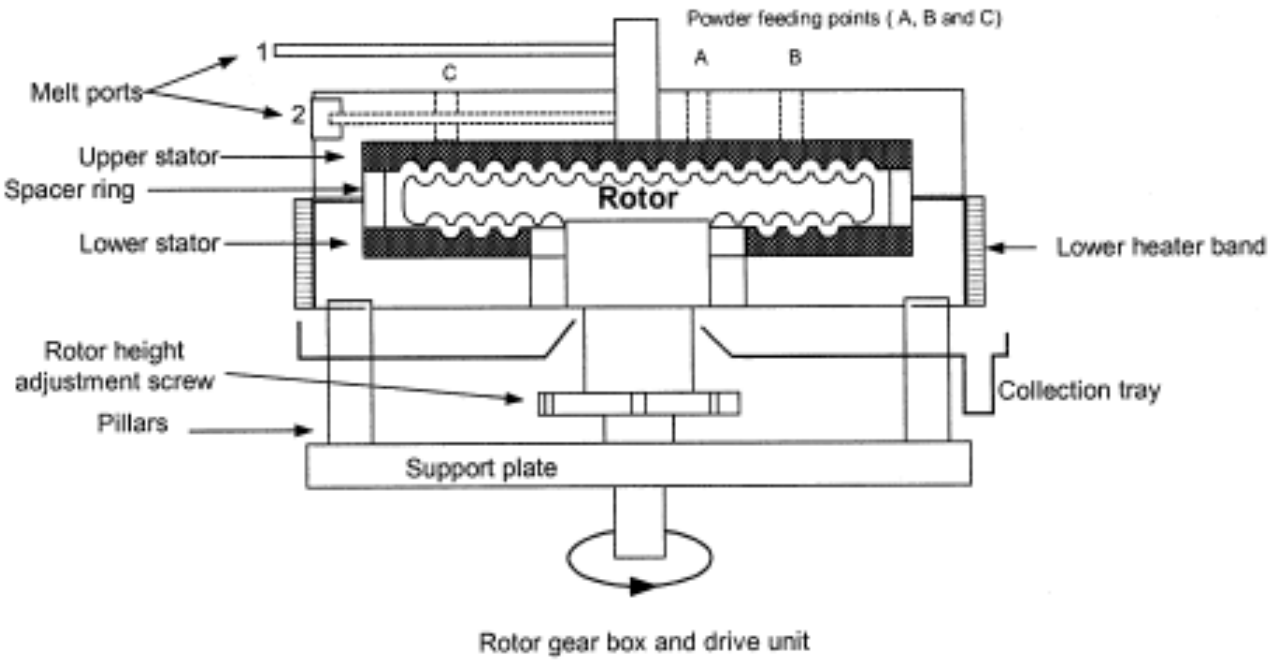

Fig. A – Diagrammatic illustration of the processing unit of the two dimensional rotating agglomerator.